

Spin-dependent surface band structure of hcp Co($\overline{10\overline{1}0}$)

Sven Bode, Kai Starke, and Günter Kaindl

*Institute of Experimental Physics and Material Science Center, Freie Universität Berlin, Arnimallee 14,
D-14195 Berlin-Dahlem, Germany*

(Received 14 October 1998; revised manuscript received 16 March 1999)

We report on a detailed analysis of the unoccupied spin-dependent surface band structure of hcp-Co($\overline{10\overline{1}0}$) using inverse photoemission with longitudinally spin-polarized electrons. At the boundary of the surface Brillouin zone \overline{Y} , an $n=1$ image-potential state is observed, which is split by 0.6 eV into an antisymmetric $n=1^-$ and a symmetric $n=1^+$ state, reflecting the high corrugation in front of the “open” hcp ($\overline{10\overline{1}0}$) surface. The upper $n=1^+$ state is nearly dispersionless in contrast to earlier predictions. Majority and minority crystal-induced surface bands, exchange split by 0.5 eV due to appreciable sd hybridization at the L_1 point of the unoccupied hcp Co band structure, exhibit almost equal effective masses. [S0163-1829(99)00127-7]

I. INTRODUCTION

Surfaces of ferromagnetic bulk single crystals have been explored extensively, driven by the search for two-dimensional magnetic behavior.¹ Early on, electronic states which are localized at the surface have been employed as probes for surface magnetization.² d -like surface states are well suited for this purpose, since they are localized in the topmost atomic layer, but unfortunately appear only in a few favorite cases.³ sp -like surface states, however exist at all close-packed metal surfaces with a *Shockley-inverted* bulk band gap.⁴

At fcc(111) metal surfaces with several-eV-wide sp band gaps near the Fermi level, so-called crystal-induced (CI) surface states are found.^{5,6} At ferromagnetic surfaces, they can contribute to the magnetic moment of the topmost atomic layer if they are *partially* occupied as with Ni(111).^{7,8} Image-potential (IP) surface states, by contrast, form a Rydberg-like series below the vacuum level and are unoccupied in the ground state; they can be accessed experimentally by inverse photoemission^{9,10} (IPE) or by two-photon photoemission.¹¹ Their wave functions have only little overlap with other electronic surface states, yet they protrude by several Å into the vacuum, giving rise to substantial tunneling probabilities.^{12,13}

While the energy position of IP states is highly sensitive to local work function changes,^{5,14} CI surface states sense details of the bulk sp band dispersion.¹⁵ The two-dimensional energy dispersion of IP and CI states, $E(k_{\parallel})$, was extensively studied by angle-resolved PE and IPE;¹⁶ most aspects of experimentally observed $E(k_{\parallel})$ relations have been well understood in the so-called phase-accumulation model which treats both Shockley-type surface states as standing waves captured between crystal surface and surface barrier.^{5,17–20}

Spin-resolved studies of Shockley states at ferromagnetic surfaces have focused on *cubic* Ni and Fe crystal lattices,^{21,22} mainly because they can be easily prepared in a single magnetic-domain state due to their higher-order anisotropy resulting in many directions of easy magnetization. Spin-polarized IPE experiments at the surface Brillouin zone (SBZ) boundaries are scarce since all other IPE spectrometers used today employ *transversely* polarized electron sources;^{23–25} they are best suited to resolve spin effects at $\overline{\Gamma}$,

where good “spin-resolution” is achieved for in-plane magnetized surfaces.

In this article we present a detailed analysis of spin-split electronic bands at the SBZ boundary of the in-plane magnetized Co($\overline{10\overline{1}0}$) surface. We utilize an IPE spectrometer equipped with a *longitudinally* spin-polarized electron source, which is optimized for large $\vec{P} \cdot \vec{M}$ at SBZ boundaries and high parallel-momentum resolution. The hcp-Co($\overline{10\overline{1}0}$) surface exhibits a large Shockley-inverted band gap at the SBZ boundary \overline{Y} , extending high above the Fermi level (E_F). At \overline{Y} , the effective vacuum energy is below the upper gap edge, giving rise to a high crystal reflectivity at energies several eV above the Fermi level. After description of the IPE spectrometer (Sec. II), and the procedure of preparing hcp-Co surfaces (Sec. III), spin-resolved IPE data are discussed in Sec. IV. Finally (Sec. V), they are described within the phase accumulation model.

II. LONGITUDINALLY SPIN-POLARIZED IPE SPECTROMETER

The longitudinally spin-polarized IPE spectrometer used here is an upgrade of the apparatus built by Grentz *et al.*²⁶ and is schematically shown in Fig. 1. Spin-polarized electrons are excited in a GaAs(001) cathode through circularly polarized light ($\lambda = 834$ nm) from a GaAlAs diode laser. A negative electron-affinity (NEA) photocathode is obtained by work function lowering via adsorption of Cs and oxygen;²⁷ for this activation the cathode is retracted into a separate UHV chamber in order to avoid contamination of the Co sample. During IPE measurements, the GaAs cathode is illuminated under 6° off normal (dotted line in Fig. 1), through an additional small hole in the Erdman-Zipf electron optics.²⁸ The performance of the gun is routinely monitored by a Faraday cup mounted on the sample manipulator; the divergence of the electron beam is below $\pm 1^\circ$ giving a spot size of 2.5-mm diameter at the sample.

Photon detection is accomplished by two bandpass counters²⁹ at different angles as shown in Fig. 1. In this way we obtain information on the light-emission characteristics which often allows a determination of the symmetry of states involved in the IPE process.³⁰ The energy bandpass is achieved through the combined effect of the excitation

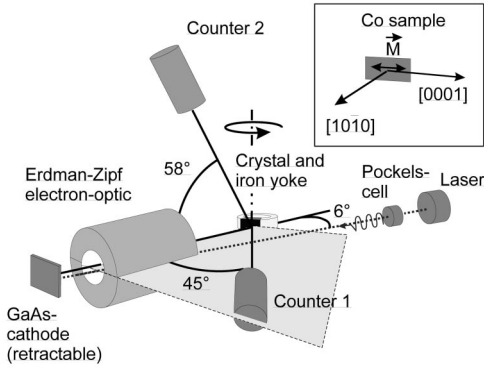


FIG. 1. Schematics of the longitudinally spin-polarized IPE apparatus. Use of two band-pass counters ($\hbar\omega=9.4\pm 0.2$ eV) at different photon-detection angles allows an analysis of light-emission characteristics. Inset: the $(10\bar{1}0)$ surface contains the Co easy axis of magnetization $[0001]$.

threshold for molecular photoionization of I_2 and the transmission cutoff of a SrF_2 entrance window; photon-detection energy is centered at 9.43 eV.³¹ The overall apparatus function, including the energy width of the electron beam, is well described by a Gaussian of 390-meV full width at half maximum (FWHM).²² A quasisimultaneous measurement of both spin directions is achieved by switching the laser-light helicity by a Pockels cell every few seconds. The degree of circular light polarization is $(96\pm 3)\%$ in the present setup, allowing for an electron-spin polarization of $\approx 30\%$.

By comparing spectra for opposite sample magnetization and opposite light helicity, we can rule out artificial spin asymmetries. A μ -metal UHV chamber and the strict use of only nonmagnetic materials (Ta, Ti, Mo, ...) near the sample results in a well-defined momentum of the low-energy electrons (kinetic energies are typically ~ 10 eV) with a parallel-momentum resolution of $k_{\parallel}/\Delta k_{\parallel} > 25$ at the SBZ boundary in the present study.

III. SAMPLE PREPARATION

Preparation of a well-ordered and chemically clean hcp $(10\bar{1}0)$ -Co single-crystal surface is an art. Due to the well-known Co hcp-fcc phase transition, cleaning recipes are restricted to moderate temperatures ($T < 700$ K). Surface and subsurface contamination is removed by soft *neon*-ion bombardment (500 eV, 4 min). Annealing the sample for 1 h at 640 K results in a well-ordered surface. Residual carbon is removed by 0.02–0.04 L oxygen exposure at $T = 580$ –600 K; residual oxygen is again removed by dosing 2-L hydrogen at $T = 640$ K. For the as-polished Co $(10\bar{1}0)$ crystal, it was necessary to repeat this cleaning cycle about a hundred times until the Auger spectrum was free of carbon and oxygen signals (below 0.02 of a monolayer equivalent).

Hydrogen gas was routinely used as a very sensitive test for a carbon-free surface region. It is well known for 3d metals that small doses of hydrogen “go subsurface” at low temperatures and force residual carbon to appear at the surfaces.^{32,33} In particular, if the Co $(10\bar{1}0)$ near-surface region contained carbon, a $C(2\times 5)$ superstructure appeared upon dosing only 0.02-L H_2 . By contrast, the clean Co $(10\bar{1}0)$ surface shows a clear $p(2\times 1)$ hydrogen super-

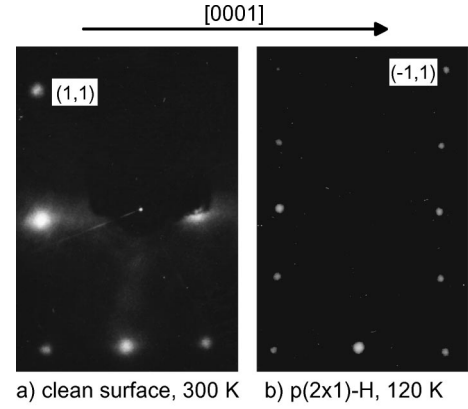


FIG. 2. LEED pictures of the Co $(10\bar{1}0)$ surface at 54 eV: (a) clean surface at $T = 300$ K; (b) H- $p(2\times 1)$ superstructure at $T = 120$ K.

structure upon ≈ 4 -L H_2 dosed at 120 K (which can be easily removed at elevated temperatures). Associate low-energy electron diffraction (LEED) images are shown in Fig. 2.

All IPE spectra were taken at room temperature, which corresponds to a reduced temperature of $t = T/T_C \approx 0.2$ ($T_C^{Co,bulk} \approx 1400$ K). Spectra were taken from the remanently magnetized sample since application of external fields during the measurement would destroy the well-defined electron parallel momentum. For spin-resolved IPE, the crystal should ideally be in a single-domain state to avoid an averaging over differently magnetized domains which can result in a cancellation of spin effects.³⁴ A common method is to use a sample geometry of closed magnetic flux. Yet hcp-Co has a large uniaxial magnetic anisotropy along the c axis, thus it is not possible to close the flux inside the crystal itself (as is frequently done for cubic crystals using a “picture-frame” geometry^{34,35}). In the present work, a *nearly* single domain state is achieved by mounting the Co $(10\bar{1}0)$ crystal in the gap of a soft-iron yoke, see Fig. 3. In order to avoid crystal stress at elevated temperatures (during the cleaning cycle), gaps of 50 μm were left between yoke and crystal. Remanence was achieved by a current pulse of ≈ 140 A applied for 1 ms to a free-hanging coil of 8 turns around the yoke. The domain state was checked *ex situ* by magneto-optical Kerr-effect (MOKE) microscopy *before* and *after* IPE experiments, see Fig. 4, as well as *in situ* by a conventional MOKE setup. Applying the “full” current of 140 A, the cobalt crystal reaches a nearly single-domain state, Figs. 4(a) and 4(b). Only near the gap between crystal and yoke, small wedge domains of opposite magnetization are formed [Fig. 4(c)] which, fortunately, do not reach the crystal center where the IPE spectra are recorded. Small stripe domains, by contrast, extend over the entire crystal surface, reducing the effective magnetization \vec{M} to $80\pm 2\%$ of the saturation \vec{M}_S . The normalized spin-signal $N_{\uparrow,\downarrow}$ is thus obtained from the measured signal $n_{\uparrow,\downarrow}$ by means of²²

$$N_{\uparrow,\downarrow} = \frac{n_{\uparrow} + n_{\downarrow}}{2} (1 \pm A), \quad (1)$$

with the spin asymmetry A

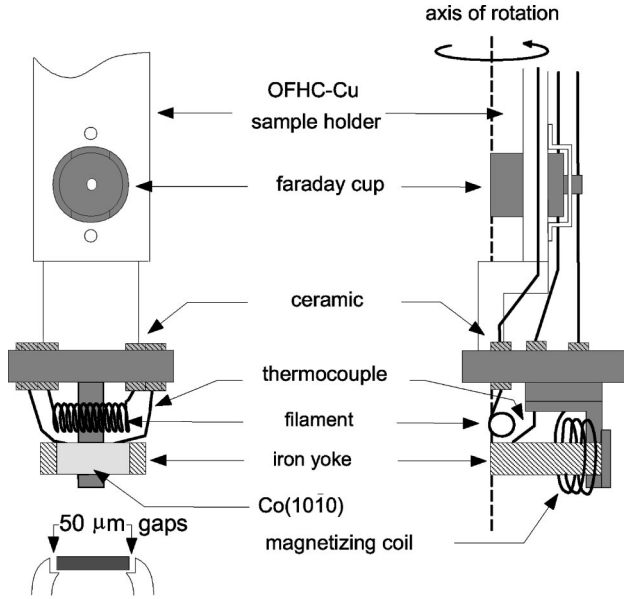


FIG. 3. Sample holder.

$$A = \frac{n_{\uparrow} - n_{\downarrow}}{n_{\uparrow} + n_{\downarrow}} \frac{1}{PM} \frac{1}{\cos \beta}, \quad (2)$$

and with $M = 0.8M_S$. β denotes the angle between electron-beam polarization \vec{P} and the average sample magnetization \vec{M} . For comparison, Fig. 4(d) shows a typical domain structure obtained after applying a too small magnetizing current (here: 70 A). It results in a “crosswalk” pattern of quite regular domains (40–70- μm width of opposite magnetization), which would cause vanishing spin effects in any spectroscopy without sufficient lateral resolution.³⁴

IV. RESULTS AND DISCUSSION

The L_1 critical points of the hcp-Co bulk bands along A - R - L define a large Shockley inverted gap at the SBZ boundary of the (1010) surface. As is shown in Fig. 5(a), it extends from about 2.2 eV up to about 7.5 eV, hereby reach-

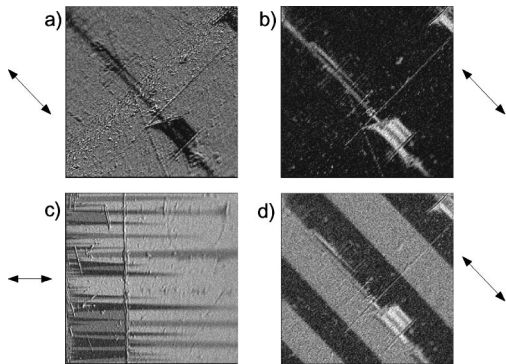


FIG. 4. *Ex situ* Kerr microscope images of the $\text{Co}(10\bar{1}0)$ crystal [(a),(b),(d): 300 $\mu\text{m} \times 300 \mu\text{m}$; (c) 1.2 mm \times 1.2 mm]. Arrows indicate the easy axis. (a) and (b) show opposite overall magnetization achieved by 140-A current pulses of opposite direction. (c) Wedge domains near the gap between crystal and yoke. (d) Stripe domains after applying 70 A.

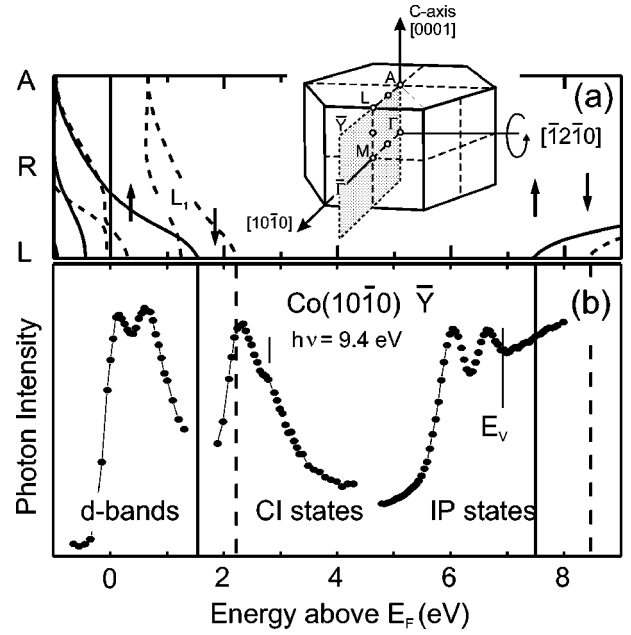


FIG. 5. (a) Calculated Co bulk band structure along A - R - L from Ref. 37, together with the reciprocal hcp lattice. Rotation of the crystal about the axis $[1\bar{2}10]$ gives access to the (gray shaded) Γ MLA azimuth. The Shockley-inverted gap is defined by L_1 points. (b) Spin-integrated spectra near \bar{Y} inside the Shockley-inverted gap (data from Ref. 38). The spin-character of the projected bulk band gaps are indicated by arrows. Note the high-energy shoulder of the crystal-induced surface state (vertical bar). E_V gives the effective electron escape energy at \bar{Y} .

ing considerably higher in energy than corresponding Shockley-inverted gaps at cubic fcc(110) surfaces. The calculation predicts sizeable exchange splittings for the lower p -like gap edge (0.67 eV) as well as for the upper s -like edge (0.86 eV),³⁶ indicating a considerable hybridization of $4sp$ bands with the exchange split $3d$ bands^{22,37} at both L_1 points. For off-normal electron motion, the effective vacuum energy, $E_{V(k_{\parallel})}$, is given by the work function Φ , plus the kinetic energy for parallel motion,

$$E_{V(k_{\parallel})} = \Phi + \frac{\hbar^2 k_{\parallel}^2}{2m}. \quad (3)$$

At the SBZ boundary of $\text{Co}(10\bar{1}0)$, E_V lies well inside the gap where surface reflectivity is high. Spin-integrated IPE spectra in Fig. 5(b) indeed reveal four significant surface structures inside the bulk band gap, which have been previously assigned^{38,39} as a spin pair of CI states near the bottom of the gap and two IP states just below E_V .

A. Crystal-induced surface bands

As a test of the surface character of the CI state, we adsorbed increasing amounts of oxygen. It is known⁴⁰ that small doses of oxygen physisorb at room temperature in a disordered and dissociated state. As shown in Fig. 6, the IPE intensity drops rapidly with increasing O_2 exposures until it is fully quenched upon 1.0 L. Alternatively, complete quenching is reached by surface roughening via soft-ion

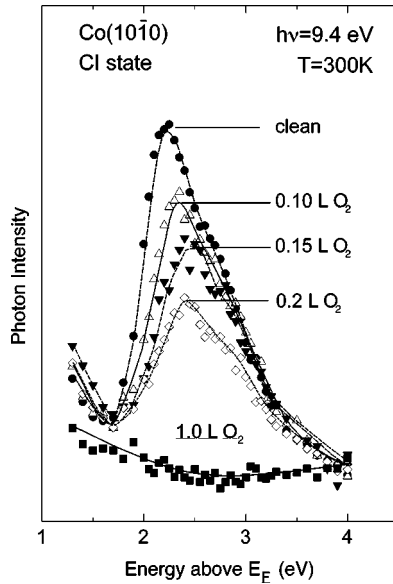


FIG. 6. Quenching of the crystal induced surface state by oxygen (lines serve as a guide to the eye).

bombardment (500-eV Ne ions for only 30 s). These observations strongly support the assignment as crystal-induced surface state.

Already the spin integrated IPE spectrum reveals a clear shoulder on the high-energy side (vertical bar in Fig. 5). Corresponding spin-resolved spectra in Fig. 7 show the existence of two CI states with opposite spin-character, which are exchange split by $\Delta E_{ex}^{n=0} = 480 \pm 50$ meV at $\bar{\Gamma}$. As was previously demonstrated, the exchange splitting of CI states gives a *lower bound* for the splitting of those bulk bands which define the gap.²² The present observation agrees well with the theoretically expected splitting of 0.67 eV for the lower gap edge.

The dispersion of the (a) majority and (b) minority CI state is presented in Fig. 8, in comparison with the calculated projected bulk band structure from Ref. 36. Peak energies are extracted from fit analyses using two different approaches: a simultaneous fit⁴¹ of (i) both spin channels recorded by one counter and of (ii) spectra from both counters and the same spin channel. The latter resulted in more precise energy positions, given in Fig. 8.

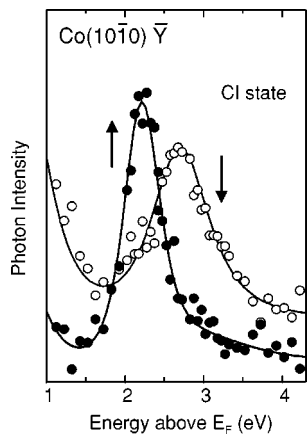


FIG. 7. Spin-resolved IPE spectra of the crystal-induced surface state at $\bar{\Gamma}$.

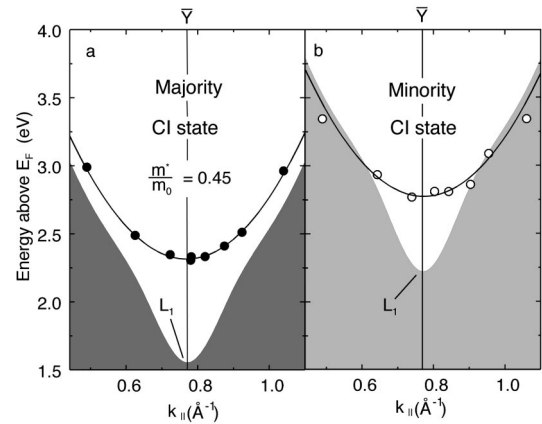


FIG. 8. Spin-resolved dispersion of the crystal-induced surface states: (a) majority spin; (b) minority spin.

Both majority and minority CI state show an upward dispersion which roughly follows the associate bulk band gaps. The majority-state dispersion can be well described by a simple parabola [solid line in Fig. 8(a)] centered at $\bar{\Gamma}$ with an effective mass

$$m^* \equiv \left. \frac{\delta^2 E(k)}{\delta k^2} \right|_{\bar{\Gamma}} \approx 0.45 m_0;$$

it thus clearly deviates from the free-electron behavior, as is generally the case when the Shockley surface-state energies are not approximately in the middle of the gap.¹⁵ Note that the experimental majority CI state energies lie inside the band gap while the minority CI state (b) crosses the gap boundaries at $\sim 0.16 \text{ \AA}^{-1}$ below and above the SBZ boundary. Near the SBZ, inside the gap, the minority state dispersion can be described by the same effective mass ($0.45 m_0$) as the majority state.⁴² The two outermost points, however, which fall into the projected bulk-band regime, deviate from the $0.45 m_0$ parabola [solid line in Fig. 8(b)]. This apparent spin dependence of the dispersion of the CI state is tentatively attributed to a stronger influence of energy-degenerate bulk bands in the minority spin case.

B. Image potential states and surface corrugation

It is well known from the concept of nearly free electrons (NFE) in bulk crystals that at Brillouin zone (BZ) boundaries, one must use linear combinations of a propagating and a Bragg reflected wave, which are either symmetric (*s*-like) or antisymmetric (*p*-like) with respect to the normal mirror plane. For a nonvanishing Fourier component V_G of the periodic bulk-crystal potential, the energy degeneracy at the BZ boundary between *p*- and *s*-like states will be lifted, opening a “partial” band gap of $2|V_G|$.

As was suggested by Smith,¹⁹ an analogous behavior may be expected for the free-electron-like Shockley surface states, which sense the two-dimensional periodicity of the crystal potential in the surface plane. In particular, at the SBZ boundary, surface states should split into pairs of $p_{||}$ - and $s_{||}$ -like symmetry, and their energy separation should be a measure of the *surface corrugation*. In earlier analyses, such “symmetry splittings” of CI surface states at Cu(110)

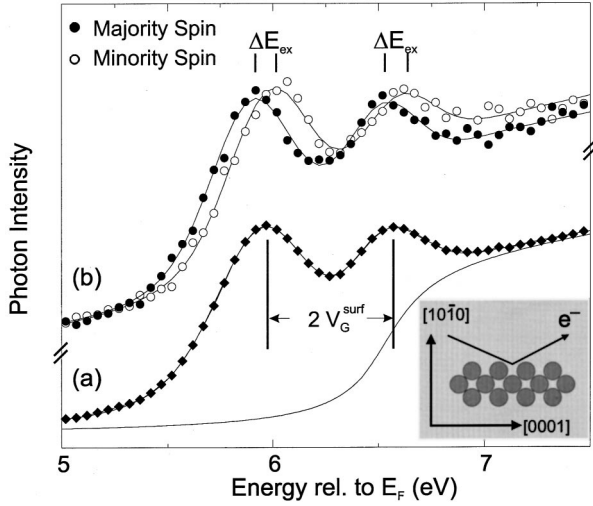


FIG. 9. Spin-integrated spectra of the $n=1$ IP states, symmetry split into an antisymmetric ($n=1^-$) and a symmetric ($n=1^+$) state. The solid line through the data (solid circles) represents the least-squares fit result. (b) Associate spin-resolved spectra of the $n=1^-$ and $n=1^+$ image state at \bar{Y} .

were found experimentally to be smaller than those predicted by a simple NFE model, suggesting some smoothing of the surface-corrugation potential in the surface layer.¹⁹

The present Co hcp-(10 $\bar{1}$ 0) surface is an “open” surface, equivalent to fcc(110). At \bar{Y} , a standing wave, resulting from incoming and Bragg-reflected partial waves, senses the largest corrugation possible at a low-Miller-indexed surface (see the inset of Fig. 9): incoming electrons move across the “rows” of the topmost layer. Figure 9(a) shows that the image-potential surface state (IP) at \bar{Y} is split by ≈ 0.6 eV into an antisymmetric $n=1^-$ and a symmetric $n=1^+$ state.³⁸ Obviously, electrons which undergo Bragg reflection a few Ångströms *in front* of the crystal still feel a substantial effective surface corrugation potential, with an associate phenomenological Fourier component $V_G^{surf} \approx 0.3$ eV. This is about 10% of the corresponding bulk corrugation potential of $V_{0002} \approx 3.3$ eV. In order to extract an exact value of the symmetry splitting at \bar{Y} , we applied a least-squares fit analysis assuming two Lorentzian peaks on an increasing background at E_V .⁴³ We simulated the principally unknown IPE background assuming various forms ranging from smoothly increasing to steplike at E_V . This procedure yields $V_G^{surf} = 305 \pm 25$ meV.

Previous experiments, also using spin-polarized IPE, demonstrated a small,²² but nonvanishing⁴⁴ spin dependence of IP state energies at Ni surfaces, which are more than one order of magnitude smaller than the average Ni 3d band exchange splitting (~ 0.3 eV). Unlike the CI state, where a shoulder is clearly discernible, the spin integrated IP spectrum in Fig. 9(a) does not indicate a spin dependence. Yet the spin-resolved IP spectra above [Fig. 9(b)] clearly show the 100-meV spin splitting of both IP states at \bar{Y} .³⁸ The observation of similarly large spin splittings for both IP states strongly supports the assignment of the upper one as an $n=1$ state, which has no nodes outside the crystal and hence a larger overlap with the exchange-split band structure of the surface layer than an $n=2$ state would have.

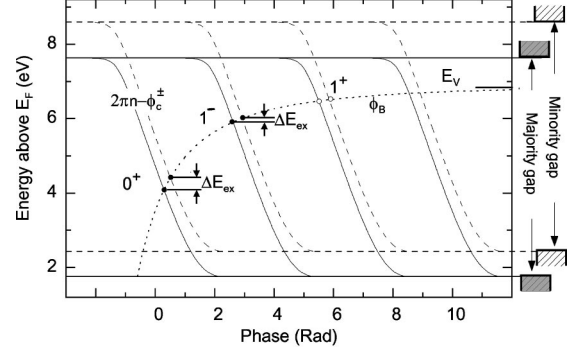


FIG. 10. Phase-accumulation-model calculation. Intersections between majority (solid) and minority (dashed) crystal phases $2\pi n - \phi_C^\pm$ and ϕ_B yield graphical solutions of Eq. (4).

V. COMPARISON WITH PHASE ACCUMULATION MODEL

For a qualitative understanding of Shockley-type surface states the phase-accumulation model (PAM) by Pendry, McRae, and Smith^{5,15,17,19,18,20,45} has frequently been used. In this model, surface states are treated as standing waves captured between the crystal surface and the surface barrier. For a $1/4z$ dependence of the image potential far outside the crystal, the model reproduces a Rydberg series of bound states with energies E_n , which are given by the phase condition for repeated reflection at the crystal and the barrier potentials:

$$\phi_C + \phi_B = 2n\pi \quad \text{with } n=0,1,2, \dots \quad (4)$$

Solutions for $n=1,2, \dots$, yield IP state energies; they are governed by the surface-barrier phase ϕ_B . By contrast, the $n=0$ solutions for CI states are mostly determined by the crystal phases ϕ_C . Following common practice, we use the two-band model for an approximate description of the energy dependence of the crystal phase $\phi_C(E)$ and the McRae formula for the barrier phase $\phi_B(E)$ (Ref. 18)

$$\frac{\phi_B}{\pi} = \left(\frac{3.4 \text{ eV}}{E_V - \epsilon} \right)^{1/2} - 1 \quad \text{for } \epsilon < E_V. \quad (5)$$

It has been shown that the surface barrier is much less spin dependent than the crystal potential, indicating that the “exchange splitting of image states is primarily a substrate effect.”⁴⁶ For a qualitative understanding of spin-dependent surface-state energies within PAM, ϕ_B may thus be regarded as non-spin-dependent.^{22,47}

To account for the symmetry doubling into symmetric (+) and antisymmetric (−) states at SBZ boundaries, Chen and Smith⁴⁸ proposed two crystal phases, ϕ_C^+ and ϕ_C^- , to be simply offset by π

$$\phi_C^+(E) = \pi + \phi_C^-(E). \quad (6)$$

Applying this suggestion to Co(10 $\bar{1}$ 0) \bar{Y} , Fig. 10 shows the crystal phases, $2\pi n - \phi_C^\pm(E)$, for majority and minority spin together with the barrier phase $\phi_B(E)$. Graphically solving Eq. (4), we find stationary state energies E_n^\pm , indicated by filled and open circles. It is evident that PAM nicely accounts for the observation of a large exchange splitting of the

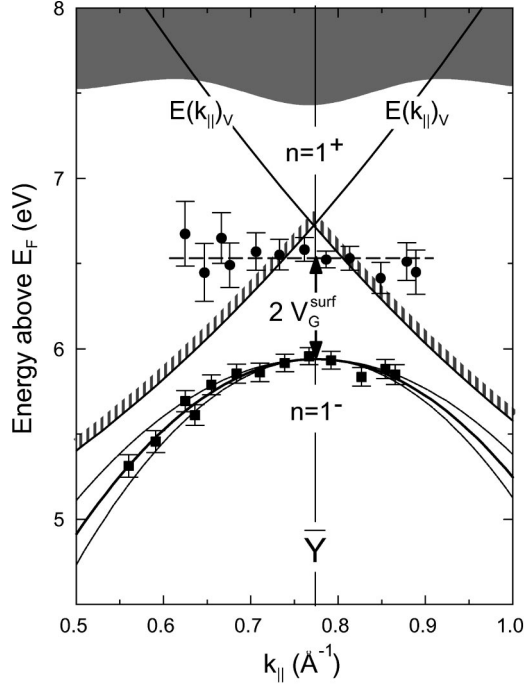


FIG. 11. Dispersion of the symmetry split $n=1^-$ and $n=1^+$ IP states. The solid line through the $n=1^-$ data gives the best parabola fit; dashed lines give the 95% confidence interval.

CI state, ΔE_{ex}^{0+} , residing in the lower part of the gap where the barrier phase is steep; they are much larger than the IP splitting because the IP intersections are close to E_V where ϕ_B diverges. Although these trends are reproduced, the model fails to account for the observed *nearly equal* spin splittings of the $n=1^-$ and the $n=1^+$ image states. This must be attributed to the somewhat artificial phase-offset introduced as a “bookkeeping trick”¹⁵ to obtain antisymmetric (1^-) and symmetric (1^+) solutions of Eq. 4 at SBZ boundaries. Hereby the $n=1^+$ spin splitting (open circles) is forced to be considerably smaller than the difference of the corresponding intersections for $n=1^-$, due to the rapidly changing slope of the barrier phase in this regime.

Deficits of PAM at SBZ boundaries become even more obvious when considering the IP dispersion, see Fig. 11. In PAM, dispersion is interpreted as resulting from the gap boundary dispersion and the concomitant changes in the crystal phase $\phi_C^\pm(E)$. The barrier phase is pinned to the effective vacuum energy

$$E_V = \phi + \frac{\hbar^2 k_{\parallel}^2}{2m},$$

which is symmetric with respect to \bar{Y} (hatched lines in Fig. 11). Electrons above the escape parabola can leave the crystal surface. Within the first SBZ, i.e., for parallel momenta $k_{\parallel} < 0.772 \text{ \AA}^{-1}$, this is possible without exchange of momentum with the crystal lattice; for larger k_{\parallel} electrons can escape via exchange of the crystal momentum $\hbar \vec{G}_{0002}$.

According to PAM, a *downward* dispersion is expected for all IP states, irrespective of their symmetry. In particular, the $E(k_{\parallel})$ bands of both $n=1$ states should always stay below the escape parabolae. Experimentally, such a downward

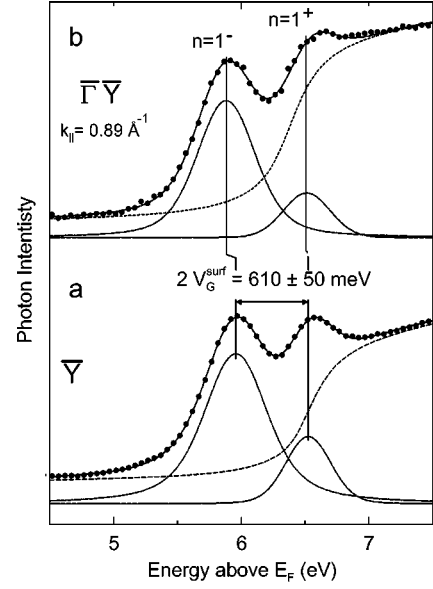


FIG. 12. Spin-integrated $n=1$ IP spectra at (a) \bar{Y} and (b) $k_{\parallel} = 0.89 \text{ \AA}^{-1}$.

dispersion is indeed found for the antisymmetric $n=1^-$ state, but clearly not for the symmetric $n=1^+$ state: It is rather stationary around \bar{Y} , for k_{\parallel} between $\approx 0.65 \text{ \AA}^{-1}$ and $\approx 0.90 \text{ \AA}^{-1}$. There is a considerable uncertainty in energy due to the principally unknown IPE background at the continuum threshold. Right at the SBZ boundary, where both $n=1$ states are visible as clear peaks [Fig. 12(a)], the energy positions cannot be far from the maxima in the IPE spectrum before background subtraction. Yet off the \bar{Y} point [Fig. 12(b)], the upper image state becomes very weak so that the energy position, as determined by least-squares fit analyses, depends on the background assumed. Yet, the experimental $n=1^+$ dispersion undoubtedly crosses the escape parabola.

The effective mass of the $n=1^-$ IP state is found to be $m^*/m = -0.28 \pm 0.04$, obviously “pinned” to the escape parabolae as was suggested by Garret and Smith.⁴⁹ The observation of an almost stationary symmetric $n=1^+$ state, by contrast, cannot be understood within the phase accumulation model and will be subject of future studies.

VI. SUMMARY

A longitudinally spin-polarized IPE spectrometer was employed for a detailed study of the unoccupied band structure of hcp Co(1010). In this spin-resolved study of a bulk single crystal of Co, a thorough analysis of the remanent domain structure ensured a reliable interpretation of spin effects. At the SBZ boundary \bar{Y} , a crystal-induced surface state is exchange split by $\approx 0.5 \text{ eV}$, nearly as large as it is theoretically expected (L_1 critical point of the hcp Co bulk band structure). A large symmetry splitting of the $n=1$ IP state at \bar{Y} reflects the strong hcp-(1010) surface corrugation which, a few \AA in front of the crystal, amounts to about 10% of the corresponding bulk corrugation. The dispersion of IP states is found to be at variance with predictions from the phase accumulation model.

ACKNOWLEDGMENTS

It is a pleasure to acknowledge the generous help of K. Christmann and P. Rech, especially in providing the Co crys-

tal and preparation recipes. We would like to thank Y.L. Gu and J. Noffke for the hcp-Co band structure calculation. This work was supported by the Sfb-290/TP-A6 of the Deutsche Forschungsgemeinschaft.

- ¹For review see, e.g., U. Gradmann, in *Handbook of Magnetic Materials*, edited by K. H. J. Buschow (Elsevier, Amsterdam, 1993), Vol. 7, p. 1.
- ²E. W. Plummer and W. Eberhardt, *Phys. Rev. B* **20**, 1444 (1979).
- ³F. J. Himpsel, *Adv. Phys.* **32**, 1 (1983).
- ⁴F. Forstmann, *Z. Phys.* **235**, 69 (1970).
- ⁵P.M. Echenique and J.P. Pendry, *J. Phys. C* **11**, 2065 (1978).
- ⁶F. Forstmann and J.B. Pendry, *Z. Phys.* **235**, 75 (1970); J.B. Pendry and F. Forstmann, *J. Phys. C* **3**, 59 (1970).
- ⁷M. Donath, F. Passek, and V. Dose, *Phys. Rev. Lett.* **70**, 2802 (1993).
- ⁸N. Memmel, *Phys. Rev. B* **55**, 5634 (1997).
- ⁹V. Dose, W. Altmann, A. Goldmann, U. Kolac, and J. Rogozik, *Phys. Rev. Lett.* **52**, 1919 (1984).
- ¹⁰D. Straub and F. J. Himpsel, *Phys. Rev. Lett.* **70**, 1922 (1984).
- ¹¹K. Giesen, F. Hage, F. J. Himpsel, H. J. Riess, and W. Steinmann, *Phys. Rev. Lett.* **55**, 300 (1985).
- ¹²G. Binnig, K. H. Frank, N. Garcia, B. Reihl, H. Rohrer, F. Salvan, and A. R. Williams, *Phys. Rev. Lett.* **55**, 991 (1985).
- ¹³O. Sánchez, J.M. Garcia, P. Segovia, J. Alvarez, A.L. Vázquez de Parga, J.E. Ortega, M. Prietsch, and R. Miranda, *Phys. Rev. B* **52**, 7894 (1995).
- ¹⁴R. Fischer, S. Schuppler, N. Fischer, T. Fauster, and W. Steinmann, *Phys. Rev. Lett.* **70**, 654 (1993).
- ¹⁵C.T. Chen and N.V. Smith, *Phys. Rev. B* **35**, 5407 (1987).
- ¹⁶A. Goldmann, V. Dose, and G. Borstel, *Phys. Rev. B* **32**, 1971 (1985).
- ¹⁷E.G. McRae, *Surf. Sci.* **25**, 491 (1971).
- ¹⁸E.G. McRae, *Rev. Mod. Phys.* **28**, 4822 (1979).
- ¹⁹N.V. Smith, *Phys. Rev. B* **32**, 3549 (1985).
- ²⁰N.V. Smith and C.T. Chen, *Surf. Sci.* **247**, 133 (1991).
- ²¹M. Donath, *Surf. Sci. Rep.* **20**, 251 (1994), and references therein.
- ²²K. Starke, K. Ertl, and V. Dose, *Phys. Rev. B* **45**, 6154 (1992).
- ²³J. Unguris, A. Seiler, R. J. Celotta, D. T. Pierce, P. D. Johnson, and N. V. Smith, *Phys. Rev. Lett.* **49**, 1047 (1982).
- ²⁴U. Kolac, M. Donath, K. Ertl, H. Liebl, and V. Dose, *Rev. Sci. Instrum.* **59**, 1933 (1988).
- ²⁵F. Ciccacci, E. Vescovo, G. Chiaia, S. De Rossi, and M. Tosca, *Rev. Sci. Instrum.* **63**, 3333 (1992).
- ²⁶W. Greutz, M. Tschudy, B. Reihl, and G. Kaindl, *Rev. Sci. Instrum.* **61**, 2528 (1990).
- ²⁷D. T. Pierce and F. Meier, *Phys. Rev. B* **13**, 5484 (1976).
- ²⁸P.W. Erdman and E.C. Zipf, *Rev. Sci. Instrum.* **53**, 225 (1982).
- ²⁹V. Dose, *Appl. Phys.* **14**, 117 (1977).
- ³⁰M. Donath, M. Glöbl, B. Senftinger, V. Dose, *Solid State Commun.* **60**, 237 (1986).
- ³¹V. Dose, T. Fauster, and R. Schneider, *Appl. Phys. A: Solids Surf.* **40**, 203 (1986).
- ³²K. Christmann, *Z. Phys. Chem., Neue Folge* **154**, 145 (1987).
- ³³M. Welz, Ph.D. thesis, Universität München, 1980.
- ³⁴K. Starke, K. Ertl, and V. Dose, *Phys. Rev. B* **46**, 9709 (1992).
- ³⁵H.J. Williams and J.G. Walker, *Phys. Rev.* **33**, 634 (1951).
- ³⁶Y.L. Gu and J. Noffke (private communication).
- ³⁷M. Donath, V. Dose, K. Ertl, and U. Kolac, *Phys. Rev. B* **41**, 5509 (1990).
- ³⁸S. Bode, K. Starke, P. Rech, and G. Kaindl, *Phys. Rev. Lett.* **72**, 1072 (1994).
- ³⁹S. Bode, K. Starke, and G. Kaindl, *J. Magn. Magn. Mater.* **148**, 183 (1995).
- ⁴⁰C. Gonser-Buntrock, Diplomarbeit, Freie Universität Berlin, 1989.
- ⁴¹In the simultaneous fit of two associate spectra only one set of spin-independent parameters was used for both spectra.
- ⁴²Parabola fits to *all* data points in Fig. 8 yield 95% confidence intervals of $m^*(\uparrow)/m_0=0.41 \dots 0.47$ and $m^*(\downarrow)/m_0=0.43 \dots 0.77$ for the majority and minority CI states, respectively. A parabola fit to data points inside the band gap yields $m^*(\uparrow)/m_0=0.468 \pm 0.015$ and $m^*(\downarrow)/m_0=0.429 \pm 0.104$.
- ⁴³The background increase is due to higher Rydberg and continuum states; it has previously been described by either a parabolic function [F.J. Himpsel, *Phys. Rev. B* **43**, 13 394 (1991)], or an arctan function [T. Watanabe, *Phys. Rev.* **139**, A1747 (1965)].
- ⁴⁴F. Passek and M. Donath, *Phys. Rev. Lett.* **69**, 1101 (1992).
- ⁴⁵N.V. Smith, *Rep. Prog. Phys.* **51**, 1227 (1988).
- ⁴⁶M. Nekovee, S. Crampin, and J.E. Inglesfield, *Phys. Rev. Lett.* **70**, 3099 (1993).
- ⁴⁷G. Borstel and G. Thörner, *Surf. Sci. Rep.* **8**, 1 (1988).
- ⁴⁸C.T. Chen and N.V. Smith, *Phys. Rev. B* **40**, 7487 (1989).
- ⁴⁹R. F. Garret and N. V. Smith, *Phys. Rev. B* **33**, 3740 (1986).